Thermochimica Acta, 230 (1993) 207–223
Elsevier Science Publishers B.V., Amsterdam
SSDI 0040-6031(93)01188-9

Thermoanalytical investigation of the formation of $YBa_2Cu_3O_{6.5}$

G.V. Rama Rao [a], P.V. Sivaprasad [a], R.K. Singh Raman [a], S. Venkadesan [a], S.L. Mannan [a,*] and U.V. Varadaraju[b]

[a] *Metallurgy and Materials Group, Indira Gandhi Centre for Atomic Research, Kalpakkam-603 102 (India)*
[b] *Materials Science Research Centre. Indian Institute of Technology, Madras-600 036 (India)*

(Received 3 March 1993; accepted 25 March 1993)

Abstract

The sol–gel process is a versatile technique generally used to obtain fine, homogeneous powders. The quality of the final product and the kinetics and mechanism by which compound formation takes place through the sol–gel process is dependent on the process parameters, such as pH, water-to-salt molar ratio and temperature of hydrolysis. In the present study, acetates of yttrium, barium and copper were employed to synthesize the high-temperature superconductor $YBa_2Cu_3O_7$ (123) by the sol–gel process. Differential thermal analysis (DTA), thermogravimetry (TG) and X-ray diffraction (XRD) techniques were employed to study the effect of pH on the kinetics and mechanism of formation of 123. The formation of 123 was found to take place either in a single step or in two steps, depending on the pH of the solution of the starting materials. The formation of 123 occurred in two steps in the samples prepared at pHs 6, 7 and 8, whereas only a single step of formation was observed in the samples prepared at pHs 6.5 and 7.5. To identify intermediate products during the formation of 123, samples were quenched at respective differential thermogravimetry (DTG) peak temperatures and characterized by XRD. Based on the kinetic analysis of the TG data, the mechanism for formation of 123 was identified as nucleation and growth following Avrami's kinetics. Samples prepared at pH 6 resulted in the formation of pure 123 compound, whereas samples prepared at other pHs resulted in impurity phases such as Y_2BaCuO_5 (211) along with 123. The activation energy for the formation of 123 was evaluated as 223 kJ mol^{-1}.

INTRODUCTION

The high-temperature superconducting compound $YBa_2Cu_3O_7$ (123) can be prepared in several ways, including the solid state, nitrate, coprecipitation and sol–gel routes, using various starting materials [1–5]. The method

* Corresponding author.

of synthesis and subsequent heat treatment schedules are of great importance in the preparation of high quality superconductors. To standardize the conditions of preparation, the study of the kinetics and the reaction mechanism of formation of 123 is essential. Šesták et al. [6] have reviewed extensively the kinetics and mechanism of both the isothermal and non-isothermal processes.

In general, kinetics and reaction mechanisms are studied both isothermally and non-isothermally by different techniques. Thermal analysis is one of the most versatile techniques used in ceramic oxide superconductor research and its application has been widely quoted since the discovery of high-temperature oxide superconductors [7–10]. Employing thermoanalytical techniques, Gaddala and Hegg [11] and Ozawa [12] reported the kinetics and reaction mechanism of formation of 123 compound prepared by the solid-state route. Kinetic studies using TG data have also been reported on the formation of 123 using various precursors such as nitrates [13], oxalates [14] and ethylhexanoates [15].

The sol–gel process is one of the most versatile techniques generally used to obtain fine, homogeneous powders [16]. The quality of the final product depends on the process parameters such as pH, water-to-salt molar ratio, and the temperature of hydrolysis [17]. In an earlier paper, we reported the effect of process parameters on the superconducting properties of 123 synthesized by the sol–gel process [18]. In this paper, we report the effect of pH on the kinetics and mechanism of formation of 123 synthesized by the sol–gel process.

EXPERIMENTAL

Gels were prepared by dissolving metal acetates of yttrium, barium and copper in 1:2:3 molar ratio in distilled water. Different samples were prepared by adjusting the pH of the metal acetate solutions to 6, 6.5, 7, 7.5 and 8 by the addition of ammonia solution. These were hydrolysed and subsequently gelled at 343 K. The preparation of the gel samples is reported elsewhere [18]. The gels thus obtained were designated A, B, C, D and E for the samples prepared at pH 6, 6.5, 7, 7.5 and 8 respectively. The gel samples were decomposed at 773 K over 12 h, followed by calcination at 1173 K over 24 h in air. The powders thus obtained were compacted at 300 MPa and subsequently sintered at 1173 K over 24 h in an oxygen environment, and cooled to room temperature at the rate of 20 K h^{-1}.

Powders were characterized by X-ray diffraction (XRD) after each heat treatment, using a Siemens 500 diffractometer with Cu Kα radiation. Differential thermal analysis (DTA) and thermogravimetry (TG) studies were carried out with a Mettler TA-1 balance with heating rate of 6 K min^{-1} to 1248 K in air. The weight of the samples used for thermal analysis experiments was in the range 40–70 mg. Particle size measurements were

carried out on the powders, obtained after grinding the sintered pellets in a mortar and pestle for ten minutes, with a Malvern E 3600 particle sizer, using the principle of light diffraction. Resistivity measurements were conducted on the sintered pellets using the Vanderpauw four-probe method.

RESULTS

Table 1 shows the phases identified by XRD in the different gel samples at various temperatures of heat treatment. It can be seen that the gel powder is amorphous at room temperature (300 K) and on heat treating at 773 K, the three phases, Y_2O_3, $BaCO_3$ and CuO, are observed. The formation of 123 compound is observed in all the samples heat treated at 1173 K for 24 h in air. Figure 1(a)–(c) shows XRD patterns of sample A (pH 6) heat treated at 1173 K for 24 h in air, and oxygenated samples of C and A treated at 1173 K for 24 h respectively. It can be concluded from Fig. 1 that pure 123 compound formation is observed in sample A, whereas the two other samples show the formation of impurity phases such as $BaCuO_2$ (011) and Y_2BaCuO_5 (211) along with 123.

The DTA plots of gels of samples A and C are shown in Fig. 2, revealing two exothermic peaks at 673 and 1153 K, and an endothermic peak at 1083 K. Similar behaviour is observed for the samples B, D and E. The DTA peak positions of all the samples are shown in Table 2.

TABLE 1

Phases identified at various temperatures in the different gel samples

Sample	Temperature in K				Particle size in μm
	300	773	1173	1173 [a]	
A	Amorphous	Y_2O_3 $BaCO_3$ CuO	123	123	1–17
B	Amorphous	Y_2O_3 $BaCO_3$ CuO	123 211	123 211	3–8 (55%) 15–27 (35%)
C	Amorphous	Y_2O_3 $BaCO_3$ CuO	123 211	123 211	3–8 (44%) 15–88 (50%)
D	Amorphous	Y_2O_3 $BaCO_3$ CuO	123 211	123 211	3–88
E	Amorphous	Y_2O_3 $BaCO_3$ CuO	123 211	123 211	3–8 (50%) 15–76 (45%)

[a] Heat-treated in oxygen.

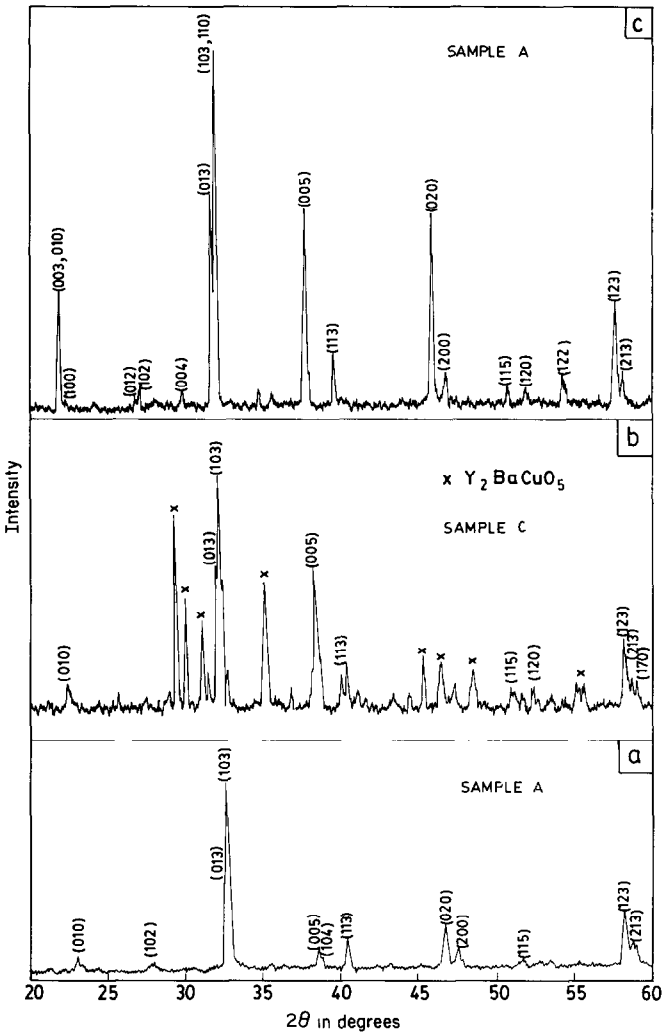

Fig. 1. XRD patterns of $YBa_2Cu_3O_7$ obtained from: (a) sample A, 1173 K for 24 h in air; (b) sample C, 1173 K for 24 h in air and 1173 K for 24 h in oxygen; and (c) sample A, 1173 K for 24 h in air and 1173 K for 24 h in oxygen.

Three regions of weight loss are observed from the TG data: a gradual weight loss up to 773 K; a plateau region up to 923 K; and a rapid weight loss up to 1223 K. The TG plots were digitized using a digitizing pad and the parameter α ($\alpha = \Delta W_T/\Delta W_\infty$), where ΔW_T is the weight loss at temperature T, i.e. the difference between the initial weight and the weight of the sample at T, and ΔW_∞ is the maximum weight loss, i.e. the difference between the initial and final weights of the sample, was evaluated. Because the formation of $BaCuO_2$ and 123 occurred in the third region of weight loss, kinetic analysis was only carried out in this region. Figure 3 shows the

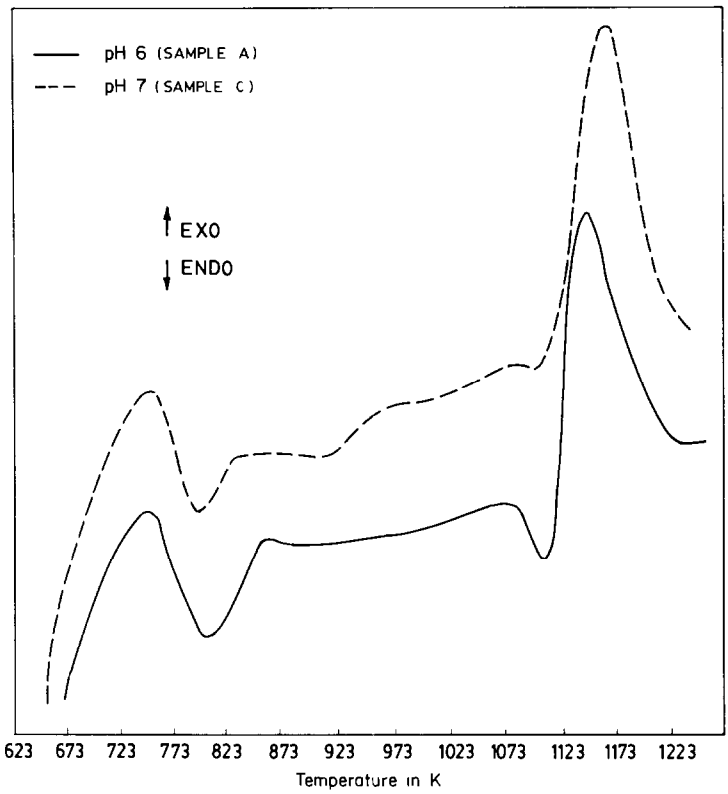

Fig. 2. DTA patterns of samples A and C.

variation of the α parameter with temperature. From this data, the differential thermogravimetry (DTG) plots were obtained for all the samples. Samples A, C and E showed that weight loss occurs in two steps leading to two DTG peaks, whereas samples B and D show a single weight loss step only (Fig. 4). To identify the intermediate compounds during the formation of 123, samples were heat treated to the corresponding temperatures of their DTG peaks, followed by air quenching. Samples thus obtained were characterized by XRD and the results are shown in Fig. 5 for sample A. The phases $BaCuO_2$, Y_2O_3, $BaCO_3$ and CuO are observed during the first DTG peak (Fig. 5(a)); formation of 123 is observed during the second DTG peak (Fig. 5(b)). The phases obtained for the other samples at their respective DTG peak temperatures are shown in Table 2. Thus it can be concluded that the first DTG peak is due to the formation of $BaCuO_2$, whereas the second peak is due to the formation of 123 (Table 2).

Particle size measurements were carried out on powder samples obtained on grinding the sintered pellets in a mortar and pestle for 10 min. The particle sizes of sample A fell in the range 2–17 μm compared to 3–70 μm for the other samples (Table 1). Resistivity (ρ) measurements showed that

TABLE 2

DTA and DTG peak positions and phases identified at DTG peak temperatures for various gel samples

Sample	Temperature in K				Phases
	DTA		Peak [a]	DTG	
	Exo	Endo			
A	693	1103	p1	1098	$BaCuO_2$, $BaCO_3$, Y_2O_3 and CuO
	1148				
			p2	1128	123
B	683	1090	p	1113	123 and 211
	1140				
C	673	1095	p1	1063	$BaCuO_2$, $BaCO_3$, Y_2O_3 and CuO
	1151		p2	1148	123 and 211
D	693	1081	p	1123	123 and 211
	1135				
E	683	1092	p1	1063	$BaCuO_2$, $BaCO_3$, Y_2O_3 and CuO
	1148				
			p2	1123	123 and 211

[a] Peaks p1 and p2 correspond to DTG peak temperatures for the formation of $BaCuO_2$ and 123, respectively; p corresponds to DTG peak temperature for the formation of 123.

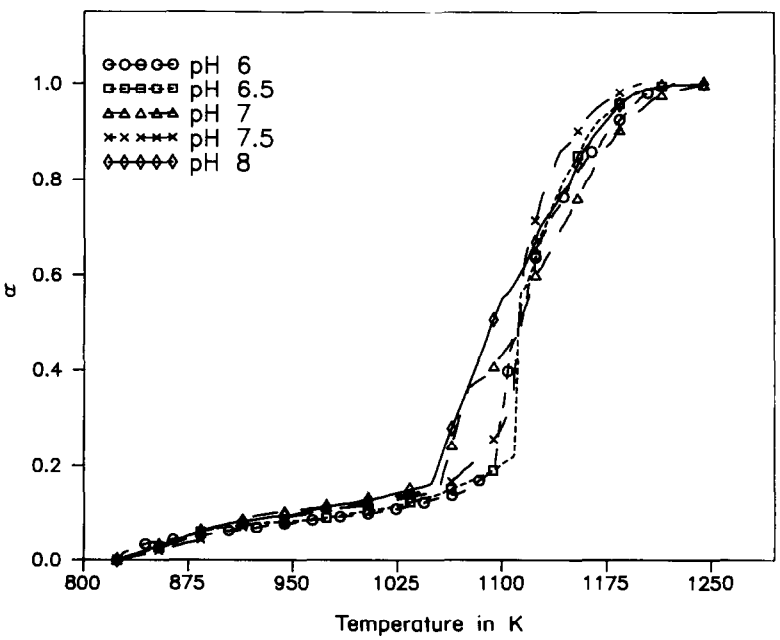

Fig. 3. The variation of the parameter α with temperature.

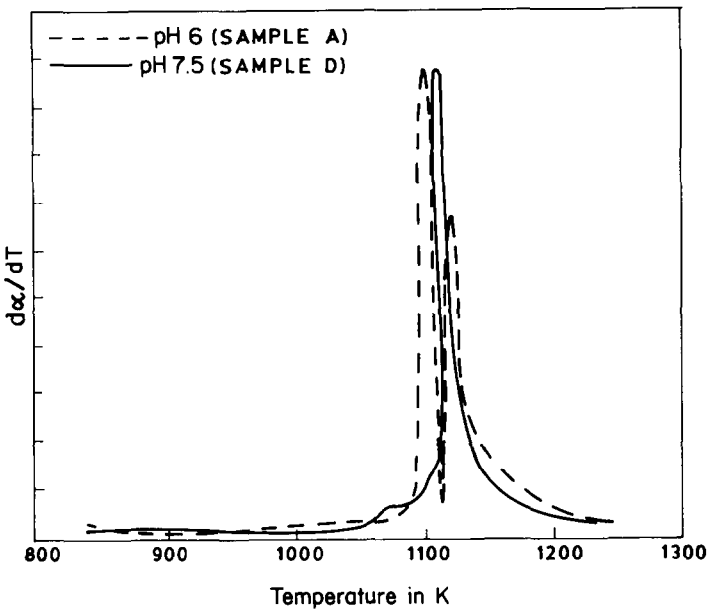

Fig. 4. DTG plots for the samples A and D.

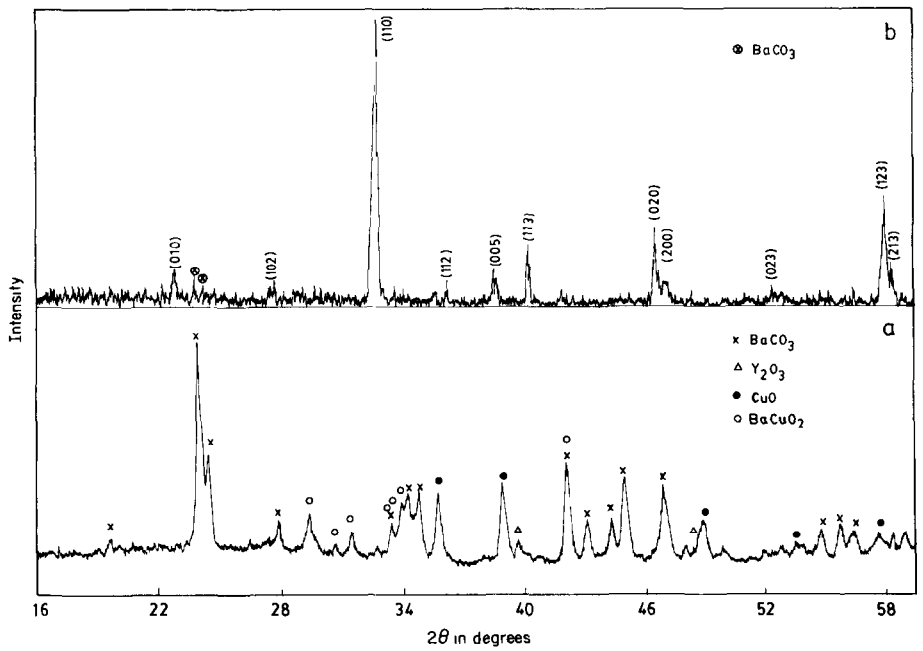

Fig. 5. XRD patterns of sample A quenched from: (a) 1098 K and (b) 1123 K.

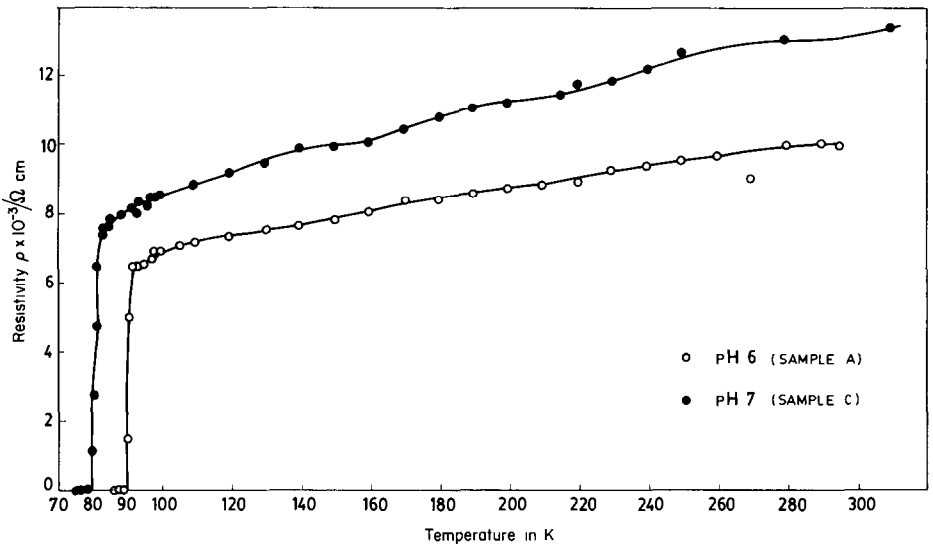

Fig. 6. Typical resistivity plots of $YBa_2Cu_3O_7$ samples.

the oxygen-treated samples of A, B, D and E exhibited the superconducting transition temperature at 90 K, whereas sample C exhibited the transition at 79 K. Figure 6 shows the $\rho-T$ plots for samples A and C. Samples B, D and E exhibited behaviour similar to that of sample A.

Reaction dynamics

The formation of 123 generally takes place with evolution of carbon dioxide, resulting in weight loss of the sample. Hence, the extent of the reaction can be expressed accurately by the weight loss ratio parameter α ($\alpha = \Delta W_T/\Delta W_\infty$). The dynamic equation for non-isothermal conditions can be generally expressed as [19]

$$\frac{d\alpha}{dT} = \frac{A}{\beta}\exp(-E/RT)f(\alpha) \tag{1}$$

where A is the frequency factor, β the heating rate, E the reaction activation energy, $f(\alpha)$ the function related to the reaction mechanism, and R and T have their usual meanings.

The difficulty in solving this dynamic equation is to determine the $f(\alpha)$ function, which first requires a knowledge of the reaction mechanism. Kinetic analysis is usually carried out by a priori assumption of the reaction

mechanism for solving the dynamic equation. This might result in a significant error in the calculation of kinetic parameters [20]. In order to overcome this difficulty, a method proposed by Phadnis and Deshpande [21] was used to identify the reaction mechanism. According to this method

$$f(\alpha)g(\alpha) = RT^2/E(\mathrm{d}\alpha/\mathrm{d}T) \tag{2}$$

where $g(\alpha) = \int \mathrm{d}\alpha/f(\alpha)$. Each reaction mechanism has a specific form of $f(\alpha)$. The functions relating to various mechanisms have to be incorporated in the above equation to generate the plots of $f(\alpha)g(\alpha)$ versus $T^2(\mathrm{d}\alpha/\mathrm{d}T)$ for the respective mechanisms. The mechanism exhibiting a linear behaviour in the above plots is considered as the mechanism responsible for the reaction process.

In the present investigation, $f(\alpha)g(\alpha)$ versus $T^2(\mathrm{d}\alpha/\mathrm{d}T)$ plots were generated for the mechanisms, namely nucleation and growth (Mampel, Avrami–Erofeev and Prout–Thompkins), diffusion (Valensi, anti-Jander and Brounshtein–Ginstling), phase boundary (two-dimensional and three-dimensional), powder law and reaction order. Figures 7 and 8 show these

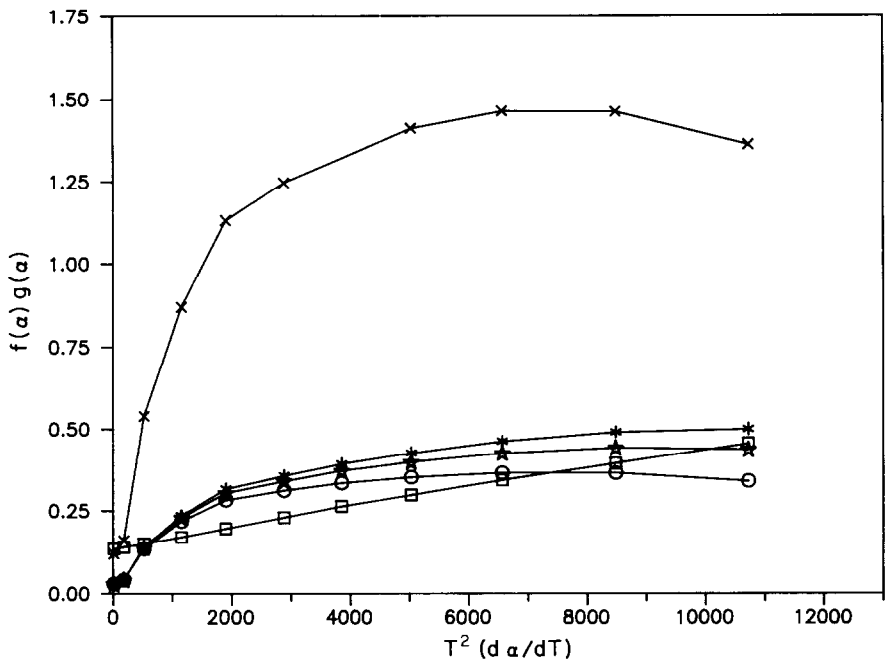

Fig. 7. Plots of $f(\alpha)g(\alpha)$ as a function of $T^2(\mathrm{d}\alpha/\mathrm{d}T)$ for different dynamic functions, $f(\alpha)$, corresponding to different reaction mechanisms during the formation of $BaCuO_2$ phase: ○, $f(\alpha) = 1 - \alpha$ (Mampel unimolecular law); ×, $f(\alpha) = 3(1-\alpha)[-\ln(1-\alpha)]^{-2/3}$ (Avrami–Erofeev nuclei and growth); □, $f(\alpha) = (1+\alpha)^{1/3}[1-(1+\alpha)^{-1/3}]^{-1}$ (anti-Jander, 3-dimensional counter diffusion); ☆, $f(\alpha) = (1-\alpha)^{2/3}$ (phase boundary contracting sphere); and *, $f(\alpha) = (1-\alpha)^{1/2}$ (phase boundary contracting cylinder).

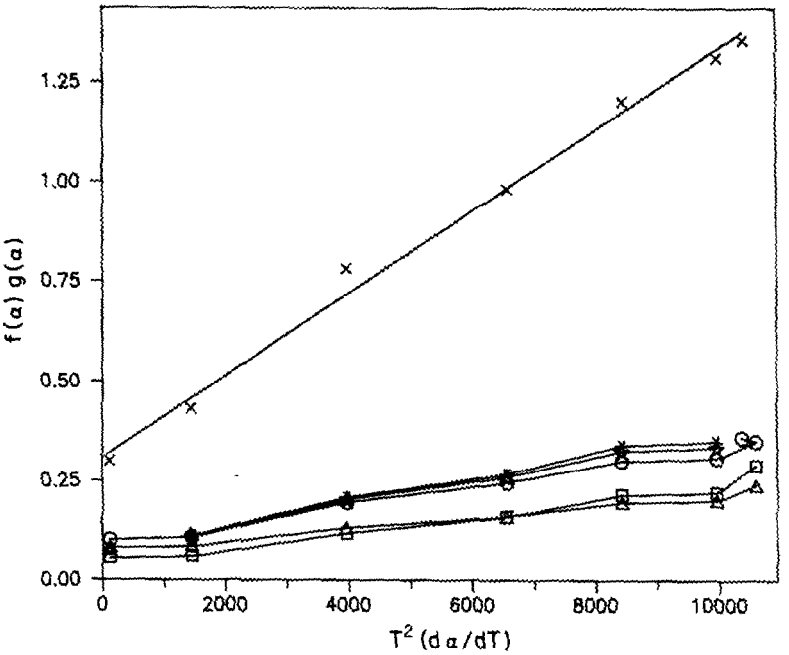

Fig. 8. Plots of $f(\alpha)g(\alpha)$ as a function of $T^2(d\alpha/dT)$ for different dynamic functions, $f(\alpha)$, corresponding to different reaction mechanisms during the formation of tetragonal 123 phase: ○, Mampel unimolecular law; ×, Avrami–Erofeev nuclei and growth; □, anti-Jander, 3-dimensional counter diffusion; △, $f(\alpha) = [(1-\alpha)^{-1/3} - 1]^{-1}$ (Brounshtein–Ginstling 3-dimensional diffusion); ☆, phase boundary contracting sphere; and *, phase boundary contracting cylinder.

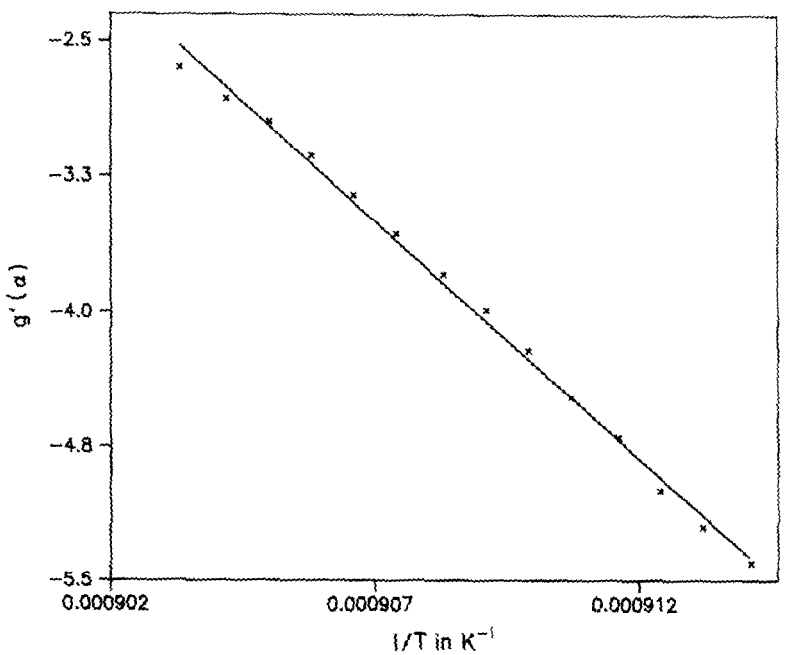

Fig. 9. Plot of $g'(\alpha) = 2\ln[(1+\alpha)^{1/3} - 1]$ as a function of $1/T$ for the formation of $BaCuO_2$.

plots for the formation of $BaCuO_2$ and 123 compounds. Figure 7 shows a linear plot for the formation of $BaCuO_2$ compound obeying an anti-Jander-type, diffusion-controlled mechanism. However, a nucleation and growth mechanism following Avrami's kinetics is found to be responsible for the formation of 123 compound (Fig. 8).

The activation energy for the above mechanisms was evaluated by the procedure described below. On integration of eqn. (2)

$$g'(\alpha) = -E/RT \tag{3}$$

where

$$g'(\alpha) = \int d\alpha / f(\alpha) g(\alpha)$$

The slope of this plot multiplied by R yields the value of E (activation energy). The $g'(\alpha)$ versus $1/T$ plots for the formation of $BaCuO_2$ and 123 compounds are shown in Figs. 9 and 10 respectively. The activation energies thus evaluated from the above plots for the formation of tetragonal 123 and $BaCuO_2$ for sample A are 223 and 950 kJ mol^{-1} respectively.

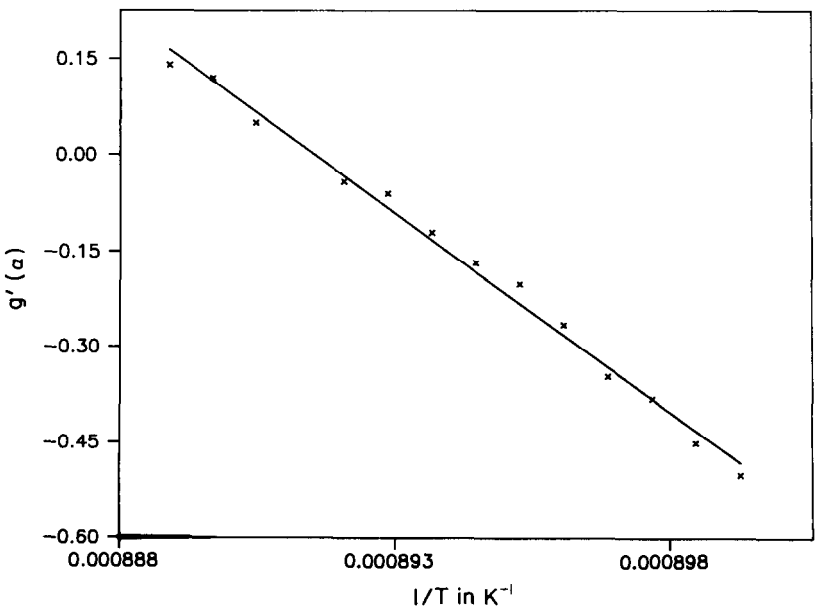

Fig. 10. Plot of $g'(\alpha) = 1/3 \ln[-\ln(1-\alpha)]$ as a function of $1/T$ for the formation of tetragonal 123 phase.

DISCUSSION

Differential thermal analysis

Before investigating the reaction between two or three solids, it is first necessary to determine how the individual materials behave on heating. This is because DTA of the reaction mixture will initially produce a curve showing a combination of all the exothermic and endothermic effects resulting from each of the materials present. Only those peaks which do not occur during the thermal excursion of the pure substances can be assigned to chemical reactions taking place between them. The exothermic peak at 673 K observed in the present study is due to the decomposition of metal acetates and the expulsion of water [22]. The other exothermic peak at 1153 K could not be attributed to any one of the starting materials, intermediate products or the final product because there was no exothermic peak reported in the range 1073–1200 K for $BaCO_3$ [23], Y_2O_3 [24], CuO [25], $BaCuO_2$ [26], $Y_2Cu_2O_5$ [26], Y_2BaCuO_5 [26] and 123 [26]. Moreover, it is reported in the literature [26] that 123 compound formation takes place in an endothermic fashion at 1233 K by the solid-state route. The partial non-crystalline nature observed in the XRD pattern of sample A quenched at 1123 K (Fig. 5(b)) suggests that the observed exothermic peak might be due to the transition of 123 from the amorphous state to crystalline state. The endothermic peak at 1083 K is due to the phase transition of $BaCO_3$ from rhombic to hexagonal [23]. The reason for the shift in the phase transition peak of $BaCO_3$ (Table 2) with variation in the pH of the samples has yet to be investigated.

Thermogravimetry

Sample A

The TG data indicated two weight-loss stages for sample A. XRD patterns at these two DTG peak temperatures confirm that the first weight loss is due to the formation of $BaCuO_2$ and that the second is due to the formation of 123. From the reaction sequences proposed for the formation of 123 compound [27], the probable reaction sequence for sample A may be suggested

1st step $$BaCO_3 + CuO \rightarrow BaCuO_2 + CO_2(g) \quad (4)$$

2nd step $$4BaCO_3 + Y_2O_3 + 6CuO \rightarrow 2YBa_2Cu_3O_{6.5} + 4CO_2 \quad (5)$$

$$4BaCuO_2 + Y_2O_3 + 2CuO \rightarrow 2YBa_2Cu_3O_{6.5} \quad (6)$$

Because there are no traces of unreacted $BaCuO_2$ in the sample heat-treated and quenched at 1123 K (second DTG peak temperature), the $BaCuO_2$ formed during the first step of the reaction would have been consumed completely in reaction (6), resuting in the formation of 123 compound. $BaCuO_2$ is formed by a diffusion-controlled mechanism, which is in agreement with that reported in the literature [28]; 123 compound is formed following Avarami's nucleation and growth model.

For sample A, 123 formation also takes place through reaction (6), but this does not result in the evolution of CO_2, i.e. there is no weight loss. Because we are monitoring the kinetics of the reaction by the parameter related to weight loss, reaction (6) cannot be explained by the mechanism proposed above.

Samples B and D

DTG data for samples B and D indicated only one weight-loss step, with DTG peak temperatures of 1113 and 1120 K respectively. XRD analysis of the samples quenched at the respective DTG temperatures revealed that, together with 123, other phases such as 211 and $BaCO_3$ are also present. It is observed from the XRD patterns that 211 phase persists even in samples heat-treated at 1173 K for 24 h in air, followed by oxygen treatment at the same temperature for 24 h (Table 1). However, the reflection peaks of $BaCO_3$ are not observed in the XRD patterns, indicating the complete elimination of $BaCO_3$. This may result from the fact that once the 211 phase is trapped inside the grains of 123, it might be very difficult for 211 to be converted to 123 [29]. Because $BaCuO_2$ is not observed in the XRD patterns, the probable reaction sequence for the formation of 123 in these samples may be proposed, together with reaction (5)

$$Y_2O_3 + BaCO_3 + CuO \rightarrow Y_2BaCuO_5 + CO_2(g) \quad (7)$$

$$Y_2BaCuO_5 + 3BaCO_3 + 5CuO \rightarrow 2YBa_2Cu_3O_{6.5} + 3CO_2 \quad (8)$$

The formation of 211 may also take place by the interaction of carbon dioxide with 123 compound following a reversal of reaction (8) [29], because the localized concentration of carbon dioxide produced by reaction (5) might increase during the course of the reaction and react with 123 to form 211 phase [29].

In these samples, both 123 and 211 phases are formed and the reactions (5) and (7) are both involved in the evolution of carbon dioxide. Therefore, using the weight loss parameter to study the kinetics of formation of 123 may not yield meaningful results. Oxygen-treated samples showed the superconducting transition onset temperature at 90 K with a ΔT_c from resistivity measurements of 5 K. The large transition width of 5 K may be the result of the presence of impurity phases. The particle sizes of samples B and D are coarser compared to that of sample A (Table 1).

Samples C and E

TG plots for these samples indicated a weight loss in two stages similar to that observed for sample A. From XRD studies, it is apparent that the first weight loss is due to the formation of $BaCuO_2$ (reaction (4)) and that the second is due to the formation of both 123 (reactions (5), (6)) and 211 (reaction (7)) phases. Table 2 shows that the formation of $BaCuO_2$ for these samples (peak 1) takes place at lower temperatures (1063 K) than for sample A (1098 K). Therefore, $BaCuO_2$ is formed earlier in samples C and E than in the others. During the second step, the rate of weight loss is slightly sluggish in the case of sample C whereas that of sample E is comparable to the other samples A, B and D (Fig. 3). The escape paths for CO_2 during its formation depend on the homogenity of the sample. The sluggishness in weight loss observed in sample C during the second stage of weight loss might be due to the incomplete escape of CO_2: $BaCuO_2$ formed during the first step might have enveloped the unreacted core, thereby slowing down the escape of CO_2 [30]. The formation of 211 impurity phase in these samples may be explained by the reasoning applied to samples B and D above. The various impurity phases found in sample C may have resulted from several side reactions, leading to conclusion that sample C is highly inhomogeneous. This may explain its lower superconducting transition onset temperature of 79 K; samples prepared at other pHs showed superconducting transition onset temperatures of 90 K. From Fig. 1(b), it can be seen that the ratio of the most intense peaks of 211 to 123 is about 70%. Even on heat treatment to higher temperatures of 1223 K for 24 h, about 20% of 211 is present as impurity phase in 123 in sample C. However, sample E heat-treated at 1173 K for 24 h yielded about 5% of 211 as impurity phase in 123. From the above discussion the probable reaction sequence for samples C and E could be predicted as reactions (4), (5), (6) and (7), together with the reaction

$$BaCuO_2 + Y_2O_3 \rightarrow Y_2BaCuO_5 \tag{9}$$

Plots of $f(\alpha)g(\alpha)$ versus $T^2(d\alpha/dT)$ for the formation of $BaCuO_2$ in samples C and E do not show linear behaviour for any of the mechanisms mentioned earlier. This suggests that the reaction processes operating for the formation of $BaCuO_2$ are quite complex for these samples. Because several side reactions are involved in the second weight-loss step, kinetic analysis was not carried out.

Sample A prepared at pH 6 yielded pure 123 compound compared to samples B, C, D and E prepared at higher pHs, namely 6.5, 7, 7.5 and 8 respectively. This may be due to the difference in bonding behaviour in the gels with respect to variation in pH. According to Kozuka et al. [2], gel formation was observed only around pH 6 in mixed metal acetate solution of yttrium, barium and copper, whereas we observed gel formation in all the samples prepared at pH 6, 6.5, 7, 7.5 and 8. Formation of the metal–oxygen–metal bond (M–O–M) during the sol–gel reaction is usually

found in hydrolysed metal alkoxide solution. The infrared absorption band below 600 cm^{-1} confirms the presence of the M–O–M bond. This absorption band is observed in samples prepared at pHs of 6.5, 7, 7.5 and 8 [18], whereas it is absent in the sample prepared at pH 6. Kozuka et al. [2] also observed that there was no M–O–M bond in the gel obtained from metal acetate solution at pH 6. Furthermore, they concluded that acetate-derived gel might consist of weakly bonded metal cation complexes and that in gel formation the acetate ions might bridge the metal cations through the two electrically negative oxygens of the –COO group [31].

In the sol–gel process, pH has a pronounced effect on the rate of the hydrolysing and condensation processes. The rate of hydrolysis is faster than that of the condensation process with increase in pH [17]. For sample A (pH 6), the rate of condensation might have been faster, thereby bridging the metal cations through the oxygens of the –COO group, leading to gel formation. However, in samples B, C, D and E of higher pH, the rate of hydrolysis would have been faster, with slower kinetics of condensation, leading to the formation of M–O–M bonds [19]. The M–O–M bond thus observed in higher pH samples could be between any two metals or between the same metal, leading to cross linking. The cross-linked network of metals might be weakly bonded to another network of metals, thereby leading to gelation. On heat treatment, the weak bonds between the networks are broken. Further decompositon of the networks would lead to the formation of inhomogeneous mixtures of oxides of yttrium, barium and copper. This inhomogeneous mixture is responsible for the impurity phases observed during the formation of 123. However, during the heat treatment of the gels of sample A, the bridges between metal cations and oxygens of the –COO group are broken and on further decomposition, homogeneous mixtures of oxides of yttrium, barium and copper are formed. This homogeneous mixture is responsible for the formation of pure 123 compound for sample A. The degree of inhomogeneities probably depends on the pH of the metal acetate solution due to inhomogeneous hydrolysis.

CONCLUSIONS

The thermoanalytical studies on the effect of pH on the formation of tetragonal $YBa_2Cu_3O_{6.5}$ by the sol–gel process have lead to the following conclusions.

(i) The sample prepared at pH 6 resulted in formation of pure 123 compound.

(ii) The sample prepared at pH 7 was highly inhomogeneous and resulted in the maximum percentage of impurity phases, resulting in a lower superconducting transition temperature of 79 K.

(iii) The steps involved in the formation of 123 and the corresponding reactions have been identified under conditions of varying pH.

(iv) The mechanisms responsible for the formation of $BaCuO_2$ and 123 compounds are identified as anti-Jander-type diffusion and Avrami nucleation and growth mechanisms, respectively.

(v) Activation energies for the formation of $BaCuO_2$ and 123 were found to be 950 and 223 kJ mol^{-1} respectively.

ACKNOWLEDGEMENTS

The authors are indebted to Dr. Placid Rodriguez, Director, Indira Gandhi Centre for Atomic Research for his constant encouragement during the course of this work. The authors also thank Dr. O.M. Sreedharan for valuable suggestions and useful discussions.

REFERENCES

1 U.V. Varadaraju and G.V. Subba Rao, in A. Narlikar (Ed.), Studies of High Temperature Superconductors, Nova Science Publishers, New York, 1989, p. 229.
2 H. Kozuka, T. Umeda, J. Jin, T. Monde and S. Sakka, Bull. Inst. Chem. Res. Kyoto Univ., 66 (1988) 80.
3 J.M. Tarascon, P.B. Barboux, B.G. Bagley, L.H. Greene and G.W. Hull, Mater. Sci. Eng., B1 (1988) 29.
4 R. Pankajavalli, J. Janaki, O.M. Sreedharan, J.B. Gnanamoorthy, G.V.N. Rao, V. Sankaara Sastry, M.P. Janawadkar, Y. Hariharan and T.S. Radhakrishnan, Physica C, 156 (1988) 737.
5 A. Douy and P. Odier, Mater. Res. Bull. 24 (1989) 1119.
6 J. Šesták, V. Satava and W. Wendlandt, Thermochim. Acta, 7 (1973) 333.
7 M. Kamimoto, Thermochim. Acta, 174 (1991) 153.
8 P.K. Gallagher, Adv. Ceram. Mater., 2 (1987) 632.
9 W.P. Brennan, M.P. Divito, R.F. Culmo and C.J. Williams, Nature, 330 (1987) 89.
10 M. Kamimoto and T. Ozawa, Thermochim. Acta, 148 (1989) 219.
11 A. Gaddala and T. Hegg, Thermochim. Acta, 145 (1989) 149.
12 T. Ozawa, Thermochim. Acta, 133 (1988) 11.
13 R.F. Zhuang, J.B. Qiu and Y.P. Zhu, J. Solid State Chem., 86 (1990) 125.
14 A. Negishi, Y. Takahashi, R. Sakamoto, M. Kamimoto and T. Ozawa, Thermochim. Acta, 132 (1988) 15.
15 A. Negishi, Y. Takahashi, R. Sakamoto, M. Kamimoto and T. Ozawa, Thermochim. Acta, 140 (1989) 41.
16 L.L. Hench and J.K. West, Chem. Rev., 90 (1990) 33.
17 G.V. Rama Rao, S. Venkadesan and V. Saraswati, J. Non-Cryst. Solids, 111 (1989) 103.
18 G.V. Rama Rao, U.V. Varadaraju, S. Venkadesan and S.L. Mannan, Proc. of DAE Solid State Physics Symposium, 34C (1991) 380.
19 C.H. Bamford and C.F.H. Tipper (Eds.), Comprehensive Chemical Kinetics, Vol. 2, Elsevier Scientific Publishing Company, Amsterdam, 1969, p. 35.
20 X.P. Jiang, J.S. Zhang, J.G. Huang, M. Jiang, G.W. Qiao, Z.Q. Hu and C.X. Shi, Mater. Lett., 7 (1988) 250.
21 A.B. Phadnis and V.V. Deshpande, Thermochim. Acta, 62 (1983) 361.
22 P. Catania, N. Hovmanian, L. Cot, M. Phamthi, R. Kormann and J.P. Ganne, Mater. Res. Bull., 25 (1990) 631.

23 M.I. Pope and M.D. Judd, Differential Thermal Analysis: A Guide to the Technique and Its Applications, Heydon and Sons Ltd., London, 1977, p. 24.
24 A.E. Miller and A.H. Daane, J. Inorg. Nucl. Chem., 27 (1965) 1955.
25 D.N. Todor, Thermal Analysis of Minerals, Abacus Press, Kent, 1976, p. 98.
26 N.L. Wu and Y.C. Chang, Thermochim. Acta, 203 (1992) 339.
27 E. Ruckenstein, S. Narain and N.L. Wu, J. Mater. Res., 4 (1989) 361.
28 A. Berlin and R.J. Robinson, Anal. Chim. Acta, 27 (1962) 50.
29 G. Selvaduray, C. Zhang, U. Balachandran, Y. Gao, K.L. Merkle, H. Shi and R.B. Poeppel, J. Mater. Res., 7 (1992) 283.
30 J. Šesták and N. Koga, Thermochim. Acta, 203 (1992) 321.
31 S. Doeuff, M. Henry, C. Sanchez and J. Livage, J. Non-Cryst. Solids, 89 (1987) 206.